Scattering by Abrupt Discontinuities on Planar Dielectric Waveguides

G. H. BROOKE AND M. M. Z. KHARADLY

Abstract—Two unifying aspects of the problem of scattering by an abrupt discontinuity on a planar dielectric waveguide are considered. The first aspect is concerned with the numerical solution of the scattering problem through consideration of a corresponding bounded waveguide problem in which perfect electric or magnetic conductor bounds with variable locations are introduced. It is shown that the solutions to the bounded problem, when numerically integrated over a range of bound locations defined within half a wavelength, allow the complete mode spectra of the unbounded waveguide to be accurately accounted for. Scattering solutions for both TE- and TM-modes are presented for a wide range of discontinuities and, in the TE-mode case, are in agreement with results obtained using the method due to Rozzi [5]. The second aspect is concerned with the relationship between scattering and "inter-waveguide mode orthogonality." Based on a simple iterative scheme, a meaningful physical interpretation of the scattering process is developed. This allows the scattering to be classified as being of first or higher order and to be explained in terms of the physical characteristics of the mode fields.

I. Introduction

DIELECTRIC surface waveguides are used in a variety of applications ranging in frequency from ultrahigh through optical. Discontinuities in cross section inevitably occur in any waveguide system due to construction tolerances and misalignment in component interconnections. In many applications, discontinuities are intentionally involved; microwave antennas and feeds and integrated optics couplers and lenses are examples.

For the purpose of analysis, it is sufficient in many cases to describe a discontinuity by an abrupt change in cross section. In other cases, it may be possible to approximate an arbitrary discontinuity by a succession of abrupt changes in the waveguide cross section. In all cases, an accurate theoretical treatment and an understanding of the scattering properties of an abrupt discontinuity are essential for the proper design of complex dielectric waveguide components and systems.

The exact solution of the discontinuity problem on an open waveguide requires that the field contributions from the continuous spectrum be specified over the infinite waveguide cross section. This results in complex spatial and spectral integrations for which exact evaluations do not appear possible. Consequently, previous investigations of the dielectric waveguide step discontinuity problem have been concerned with approximate solution techniques (e.g., [1]–[4]). These techniques are limited to various degrees in the scope of their applicability. Basically, this is due to the manner in which the continuous spectrum of modes on the unbounded waveguide is treated. More recently, Rozzi [5] has described a new technique which employs Laguerre polynomials in a Ritz–Galerkin variational solution and which has been successfully applied to TE-mode scattering by a step on a planar dielectric waveguide. This solution technique does not appear to be as readily applied to the TM-mode case, however.

The approach presented in this paper circumvents some inherent difficulties associated with the previous methods and it is applicable to dielectric waveguides having arbitrary permittivity and to step discontinuities of any size. Essentially, by maintaining a direct relationship to modal quantities, it is mathematically less complex, provides some insight into the scattering process and, finally, is as easily applied to TM- as it is to TE-mode scattering. The basis of the present approach is the reduction of the unbounded (original) problem to a bounded (modified) problem where the open structure is enclosed by perfect electric or magnetic conductors. The solution to the original problem is then extracted from that of the corresponding modified problem [6], [7]. This process leads to the development of a simple and accurate numerical technique for solving the discontinuity problem in the "variable-bound" approach and of a simple and meaningful interpretation of the scattering process.

The main points discussed in this paper include: a) the limitations of the straightforward bounding procedure applied hitherto; b) the procedures necessary to fully and accurately account for the continuous spectrum; c) the relationships between the scattering process and mode orthogonality; and d) the characteristics of TE- and TM-mode scattering over a wide range of discontinuities.

II. The Bounded Approach

The bounded approach involves bounding the dielectric waveguide with either perfect electric (E-bound) or perfect magnetic (H-bound) conductors, as shown in Fig. 1, and then solving the bounded problem using mode matching. Because of the one-to-one correspondence of the mode spectra of the bounded and unbounded configurations, the

Manuscript received April 28, 1981; revised November 4, 1981. This work was supported by the National Research Council of Canada, under Grant A-3344.

G. H. Brooke is with the Defence Research Establishment (Pacific), FMO Victoria, British Columbia, Canada V0S 1B0.

M. M. Z. Kharadly is with the Department of Electrical Engineering, University of British Columbia, Vancouver, British Columbia, Canada V6T 1W5.

0018-9480/82/0500-0760$00.75 ©1982 IEEE

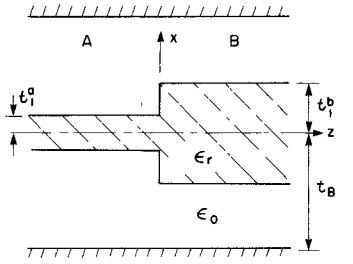

Fig 1. Bounded waveguide discontinuity configuration.

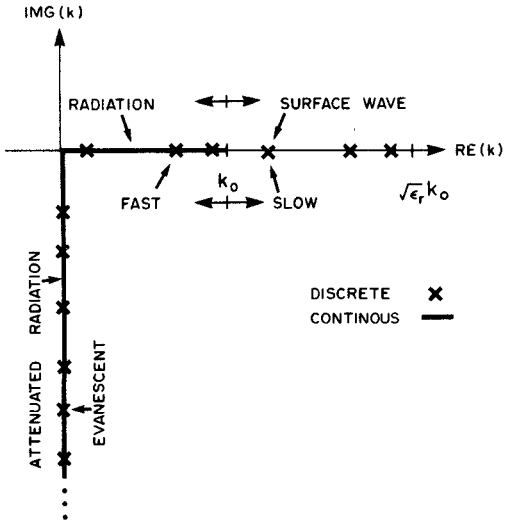

Fig. 2. Mode spectra in the k-plane.

solution for the bounded problem provides an approximate solution of the original problem. A k-plane representation of the mode spectra for the two configurations is shown in Fig. 2. For the bounded configuration, the modes in the spectral ranges $k_0 \leqslant \beta \leqslant \sqrt{\epsilon}_r k_0$, $0 \leqslant \beta \leqslant k_0$, and $-j\infty < \beta < -j0$ are usually referred to as slow, fast, and evanescent, respectively, whereas in the unbounded configuration the corresponding modes are referred to as surface wave, radiation, and attenuated radiation, respectively [7]. In the above, β is the propagation coefficient, $k_0 = 2\pi/\lambda_0$ is the free-space wavenumber and ϵ_r is the relative permittivity of the dielectric.

A summary of the functional form of the modes in a uniform waveguide (either waveguide A or waveguide B in Fig. 1) is given in Table I for TE-modes (H-bound) and in Table II for TM-modes (E-bound).

In the above tables, $p_1 = (\epsilon_r k_0^2 - \beta^2)^{1/2}$ and $p_2 = (k_0^2 - \beta^2)^{1/2}$ are the transverse propagation coefficients, η_0 is the intrinsic impedance of free space, and $F_E(\beta)$ and $F_M(\beta)$ are the characteristic equations of the structure for TE- and TM-modes, respectively. The correspondence between the fields of the bounded and unbounded configurations is examined in Appendix I. The analysis indicates that the fast and the evanescent modes are functionally identical to the continuous spectrum modes at discrete values of β (defined by solutions of $F_E(\beta)$ or $F_M(\beta)$ in the appropriate spectral ranges), whereas the slow and the surface wave modes become functionally identical in the limit as $t_B \to \infty$. In practice, however, t_B need only be a few free-space wavelengths for the slow and the surface wave modes to exhibit virtually identical behavior.

TABLE I
TE-MODE FIELDS AND CHARACTERISTIC EQUATIONS $F_E(\beta)$: (H BOUND)

$\lvert t\rvert \leq t_1$	e_y	$\cos p_1 x$
	h_x	$-\frac{\beta}{k_0\eta_0}\cos p_1 x$
	h_z	$-\frac{jp_1}{k_0\eta_0}\sin p_1 x$
$t_1 \leq \lvert t\rvert \leq t_B$	e_y	$C\cos p_2(x - t_B)$
	h_x	$-\frac{C\beta}{k_0\eta_0}\cos p_2(x - t_B)$
	h_z	$-j\frac{Cp_2}{k_0\eta_0}\sin p_2(x - t_B)$
	C	$\cos p_1 t_1 / \cos p_2(t_1 - t_B)$
$F_E(\beta)$		$p_1 \tan p_1 t_1 = p_2 \tan p_2(t_1 - t_B)$

TABLE II
TM-MODE FIELDS AND CHARACTERISTIC EQUATION $F_M(\beta)$: (E BOUND)

$\lvert t\rvert \leq t_1$	h_y	$\cos p_1 x$
	e_x	$\frac{\beta\eta_0}{k_0\epsilon_r}\cos p_1 x$
	e_z	$j\frac{p_1\eta_0}{k_0\epsilon_r}\sin p_1 x$
$t_1 \leq \lvert t\rvert \leq t_B$	h_y	$C\cos p_2(x - t_B)$
	e_x	$\frac{C\beta\eta_0}{k_0}\cos p_2(x - t_B)$
	e_z	$j\frac{Cp_2\eta_0}{k_0}\sin p_2(x - t_B)$
	C	$\cos p_1 t_1 / \cos p_2(t_1 - t_B)$
$F_M(\beta)$		$p_1 \tan p_1 t_1 = \epsilon_r p_2 \tan p_2(t_1 - t_B)$

The correspondence of the slow and surface wave modes is an important factor affecting the implementation of the bounded approach and, hence, will be illustrated by examining the value of the propagation coefficient β as a function of t_B. Consider an example in which $\epsilon_r = 5.0$ and $t_1 = 0.01\lambda_0$. Fig. 3 gives plots of the ratio of the propagation coefficients of the slow and of the surface wave modes versus $(t_B - t_1)/\lambda_0$ for each type of mode with each type of bound. The graphs for TE- (E-bound) and for TM- (H-bound) modes exhibit a cutoff behavior and thus suggest that for these mode types the respective bounds are, in general, inappropriate. More appropriately, however, the graphs for TE- (H-bound) and for TM- (E-bound) modes exhibit no low-frequency cutoff and also indicate that the

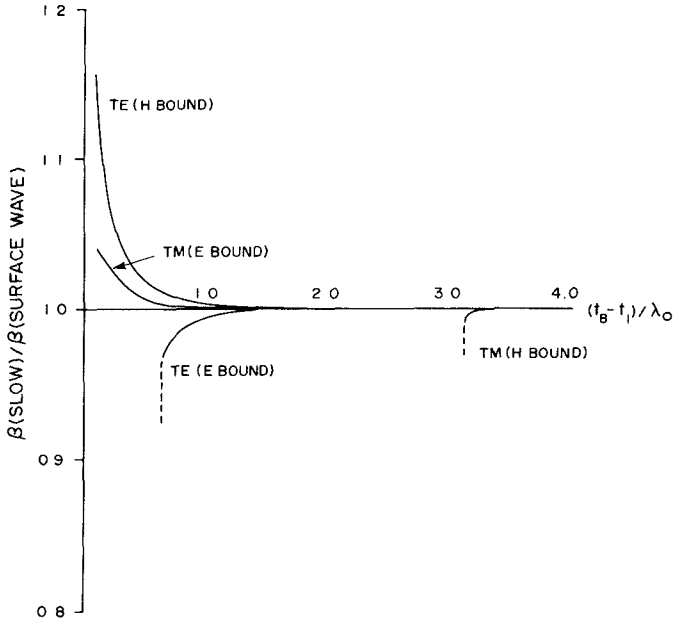

Fig 3 Ratio of slow to surface wave mode propagation coefficients against $(t_B - t_1)/\lambda_0$: $\epsilon_r = 5.0$, $t_1 = 0.01\lambda_0$.

values of the slow-mode propagation coefficients do not differ significantly from those for the corresponding surface wave modes over a wider range of $(t_B - t_1)/\lambda_0$.

It may be noted that in the above example the surface wave mode is relatively loosely bound to the dielectric. As ϵ_r or t_1 is increased, there will be even less discrepancy between the values of β for much smaller values of $(t_B - t_1)/\lambda_0$, except for higher order slow modes close to cutoff.

A. Mode Matching

Referring to Fig. 1, the transverse electric and magnetic field vectors are denoted by $\boldsymbol{e}$ and $\boldsymbol{h}$, respectively. Let a mode of unit amplitude be incident from waveguide A. The mode-matching equations in the plane of the discontinuity may be written as

$$\boldsymbol{e}_i^a + \sum_{n=1}^{\infty} a_n \boldsymbol{e}_n^a = \sum_{m=1}^{\infty} b_m \boldsymbol{e}_m^b \tag{1}$$

$$\boldsymbol{h}_i^a - \sum_{n=1}^{\infty} a_n \boldsymbol{h}_n^a = \sum_{m=1}^{\infty} b_m \boldsymbol{h}_m^b. \tag{2}$$

In the above equations, the subscript i denotes the incident mode, and superscripts a and b denote waveguides A and B, respectively. The expressions for the fields in (1) and (2) can be found in Table I or Table II.

In order that solutions for the scattering coefficients $\{a_n, b_n\}$ may be obtained, the infinite sums in (1) and (2) are truncated. In this work, equal numbers of modes N are used to approximate the fields on either side of the discontinuity, as has been established in [8]. The conventional approach [9] to solving (1) and (2) is to use the orthogonality relations between the modes given by

$$\int_0^{t_B} \boldsymbol{e}_k^a \times \boldsymbol{h}_i^a \cdot \boldsymbol{a}_z \, dx = \delta_{ki} P_k^a \tag{3}$$

$$\int_0^{t_B} \boldsymbol{e}_k^b \times \boldsymbol{h}_i^b \cdot \boldsymbol{a}_z \, dx = \delta_{ki} P_k^b \tag{4}$$

to obtain

$$\sum_{m=1}^{N} b_m \left(P_{mk}^{ba} + P_{km}^{ab} \right) = 2\delta_{ki} P_i^a \tag{5}$$

and

$$a_k = \delta_{ki} - \sum_{m=1}^{N} b_m \frac{P_{km}^{ab}}{P_k^a}, \qquad k = 1, \cdots, N \tag{6}$$

where δ is the Kronecker delta and

$$P_{mk}^{ba} = \int_0^{t_B} \boldsymbol{e}_m^b \times \boldsymbol{h}_k^a \cdot \boldsymbol{a}_z \, dx \tag{7}$$

$$P_{km}^{ab} = \int_0^{t_B} \boldsymbol{e}_k^a \times \boldsymbol{h}_m^b \cdot \boldsymbol{a}_z \, dx. \tag{8}$$

The relations in (7) and (8) describe the "inter-waveguide orthogonality" of the modes for which explicit expressions are given in Appendix II. Expressions for P_k^a and P_k^b are also given in Appendix II. Thus, the mode coefficients $\{b_m\}$ are obtained by solving the linear system of (5) and the mode coefficients $\{a_n\}$ are obtained by substitution into (6).

It is appropriate at this point to define a set of normalized mode coefficients as follows:

$$\bar{a}_n = a_n \left(P_n^a / P_i^a \right)^{1/2} \tag{9}$$

$$\bar{b}_m = b_m \left(P_m^b / P_i^a \right)^{1/2}, \qquad m, n = 1, \cdots, N. \tag{10}$$

These coefficients may be used to obtain a useful check on the mode-matching solutions—the power conservation error P_e being given by

$$P_e = 1 - \sum_{n=1}^{N_p^a} |\bar{a}_n|^2 - \sum_{m=1}^{N_p^b} |\bar{b}_m|^2 \tag{11}$$

where N_p^a and N_p^b are the total numbers of propagating modes in waveguides A and B, respectively. Furthermore, the relative power contained in the fast modes is given by

$$P_r = \sum_{n=N_s^a+1}^{N_p^a} |\bar{a}_n|^2 + \sum_{m=N_s^b+1}^{N_p^b} |\bar{b}_m|^2 \tag{12}$$

where N_s^a and N_s^b are the numbers of slow modes in waveguides A and B, respectively. As will be illustrated in Section III, the value of P_r is an approximation to the normalized radiated power in the original problem. In the discussion and analysis to follow, coefficients $\{a_n\}$ and $\{b_m\}$ will be conventionally associated with waveguides A and B, respectively.

B. Accuracy of Solutions

The accuracy of the solution of the modified problem, as an approximation to the solution of the original problem, depends mainly upon two factors; namely, the bound location t_B and the number of modes N. It will be shown that the value of N required for a certain accuracy will, in general, depend on the choice of t_B. The effect of these factors will be demonstrated by considering a numerical example ($\epsilon_r = 5.0$, $t_1^a = 0.07\lambda_0$, and $t_1^b = 0.35\lambda_0$) in which the second slow mode from waveguide B is incident. This mode has been chosen because its behavior is typical of

TABLE III
DEPENDENCE OF THE SOLUTIONS ON N

	$t_{Bo} = 2.0$			$t_{Bo} = 4.0$		
N	$\lvert b_2\rvert$	$\angle b_2$	P_e	$\lvert b_2\rvert$	$\angle b_2$	P_e
5	.4237	0	.5974	.2203	0	8.58
10	.4050	.5164	.0136	.4444	.2678	.2330
15	.4081	.5490	.0013	.4299	.549	.0132
20	.4081	.5537	.0002	.4265	.5604	.0130
25	.4081	.5541	2×10^{-5}	.4286	.5770	.0061
30	.4082	.5545	2×10^{-5}	.4294	.5934	.0009
40	.4082	.5546	1×10^{-5}	.4294	.5961	.0001

cases in which the scattering solutions of the bounded problems are sensitive to the bound location. In order that a comparison with the results obtained using Rozzi's method may eventually be made, TE-mode propagation is discussed.

1) The Dependence on N: The effect of N can be deduced by computing the solution of the above example for two different values of t_B and by observing the behavior of the solutions as a function of the number of modes. The results are summarized in Table III where the reflection coefficient b_2 of the incident mode is tabulated for various values of N and for each value of $t_{B0} = t_B/\lambda_0$. The corresponding values of P_e are also given in this table.

The above results are typical of the convergence as a function of N. It may be noted that faster convergence occurs for the smaller value of t_{B0}. These results, which imply that higher order modes are excited more readily as t_{B0} increases, may be explained as follows. The excitation of the high-order evanescent modes depends on the inter-waveguide orthogonality of these modes with respect to the low-order slow modes and, hence, is related to the transverse field behavior of the modes in the range $t_1 \leq |x| \leq t_B$; in this range, the slow modes have no phase reversals whereas the evanescent modes have approximately M phase reversals (M is the mode order). Accordingly, from stationary phase arguments, the high-order modes tend to be orthogonal to the low-order modes as M becomes large. However, as t_{B0} increases, the Mth mode tends to be less orthogonal to the slow modes because the M phase reversals are now more dispersed along the x coordinate.

An important feature of the results shown in Table III is the different value of b_2 to which the solution converges for different values of t_{B0}.

2) The Dependence on t_B: The magnitude of b_2, in the previous example, is plotted versus t_{B0} in Fig. 4. These results were calculated with $N = 40$[1] to achieve a value of P_e less than 0.5 percent over the range of large t_{B0}. The oscillating value of $|b_2|$ appears to have the following properties: i) a period of oscillation equal to 0.5; ii) a constant mean value; and iii) a slow rate of convergence. These properties may be qualitatively explained by considering the dispersion characteristics of the modes as functions of t_{B0}. Fig. 3 shows that the dispersion of the slow modes is slight for practical values of t_{B0} and diminishes with increasing t_{B0}. The normalized propagation coefficients β/k_0 of the fast-modes in waveguide B are shown in Fig. 5 as a function of t_{B0}. It is evident that these modes are highly dispersive over the lower part of the spectrum and consequently there is an uneven density of modes in the range $0 \leq \beta \leq k_0$, as illustrated in Fig. 5 at $t_{B0} = 4$. Further analysis indicates that the evanescent modes are also highly dispersive but that their density over the range $-j\infty \leq \beta \leq -j0$ is nearly uniform. The oscillations are attributed to the effect of the variable density of modes over the fast-mode spectrum and, hence, to their variable contribution to the scattering solutions. The period of the oscillation is thus a result of the transition of an evanescent mode into the fast-mode spectrum at regular intervals of 0.5 in t_{B0} (as shown in Fig. 5 and as predicted by consideration of $F_E(\beta)$ in Table I). The oscillation appears to be about a constant mean value because the slow modes, in

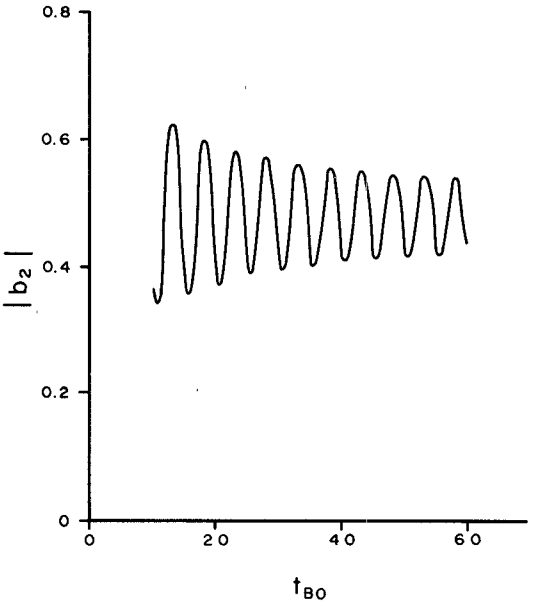

Fig. 4. Magnitude of the slow-mode reflection coefficient $|b_2|$ against t_{B0}: $\epsilon_r = 5.0$, $t_1^a = 0.2t_1^b$, $t_1^b = 0.35\lambda_0$.

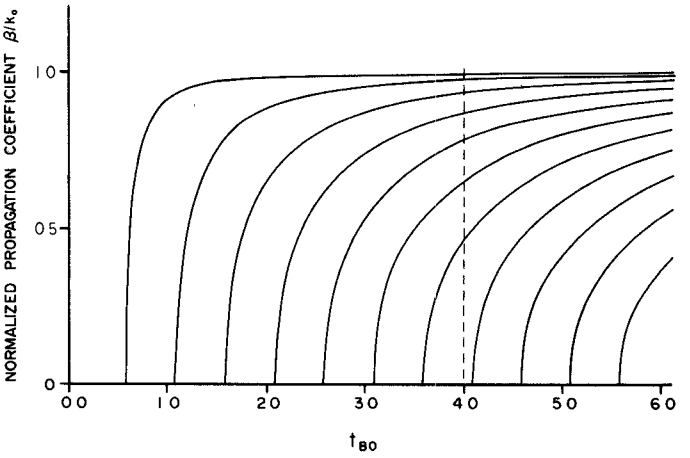

Fig. 5. Fast-mode dispersion characteristics as a function of t_{B0}: $\epsilon_r = 5.0$, $t_1 = 0.35\lambda_0$.

[1]For convenience, this large value of N was used over the whole range, although the results in the previous section indicate that this was not necessary.

this case, are only slightly and diminishingly dependent on t_{B0}. In general, the oscillation is not necessarily about a constant mean value but for sufficiently large values of t_{B0}, this appears to be a valid approximation. The final property, slow convergence, is due to the relatively slow increase in the density of fast modes in the lower part of the fast-mode spectrum.

All slow-mode scattering coefficients exhibit a dependence on t_{B0}. The magnitude of the oscillations will depend, however, on the relative excitation of the lower part of the fast-mode spectrum.

At this point, it may be appropriate to interpret the above properties of slow-mode scattering solutions in the context of the bounded approach. By referring to Fig. 2, one may recall that in this approach the fast and evanescent modes provide a means of treating the continuous spectrum approximately. In the present numerical example the approximation is highly dependent on t_{B0} because a significant amount of energy in the corresponding unbounded problem is scattered into the lower part of the spectral range $0 \leq \beta \leq k_0$. The relatively poor coverage of this part of the spectrum by the fast modes is therefore accentuated. In theory, this problem may be overcome by increasing t_{B0} and thereby improving the coverage provided by the fast modes. In practice, however, the slow convergence of the oscillations make the required value of t_{B0} and, hence, N (Section II-B-1) so large that the problem becomes numerically untractable.

The above discussion points out the limitations of the straightforward application of the bounded approach, in which the approximate solution to the unbounded problem is obtained using a single value of t_{B0}. That is, the accuracy of this approach is limited whenever the lower part of the spectral range $0 \leq \beta \leq k_0$ is well excited. A simple modification, however, suggested by the second property of the slow mode coefficients (i.e., oscillation about a mean value), allows all cases to be accurately dealt with, as will be discussed in the following sections.

C. A Variable-Bound Approach

The apparent oscillation of the slow-mode scattering coefficients about a constant mean value suggests that the limiting value of the oscillations (the desired solution) may be approximated by estimates of these mean values. In the variable-bound approach, these estimates are obtained by simply averaging the scattering coefficients over a single period $\Delta t_{B0} = 0.5$. This amounts to a rectangular numerical integration. The results for the previous example, for various choices of Δt_{B0}, are summarized in Table IV, where an averaging interval δt_{B0} of 0.1 is used. Corresponding results obtained by applying Rozzi's method [5] to the original problem are also presented in this table. These are denoted by R_6 and R_{10} for six and ten terms in the Laguerre polynomial expansion, respectively.

The above results confirm the second property discussed in the previous section, namely, that the mean value of the oscillations is not a constant, but for t_{B0} sufficiently large, it is approximately so. They also confirm that an accurate approximation (by comparison with Rozzi's results) to the limiting value of the oscillations may be obtained by estimating the mean value. Generally speaking, the estimates can be calculated over a range Δt_{B0} in which $(t_B - t_1)/\lambda_0$ is of the order of one or two and, therefore, the value of N required to achieve reasonable accuracy is numerically acceptable.

TABLE IV
INTEGRATED SCATTERING COEFFICIENTS

Δt_{B0}	$\lvert\bar{a}_1\rvert$	$\lvert\bar{b}_1\rvert$	$\lvert\bar{b}_2\rvert$
0.9-1.4	0.3258	0.1765	0.4728
1.9-2.4	0.3262	0.1795	0.4790
3.9-4.4	0.3280	0.1819	0.4813
R_6	0.3282	0.1834	0.4940
R_{10}	0.3272	0.1814	0.4820

Thus, by numerically integrating the solutions obtained over a small range of bound locations, the variable-bound approach yields accurate approximations to the solutions of the original unbounded problem. The results of other examples are presented in Section III.

D. Summarizing Remarks

The solution of either the original (unbounded) or the modified (bounded) discontinuity problem requires all components of the complete spectrum to be accurately accounted for. In the original problem, this requires that a difficult integration over the continuous spectrum be performed whereas, in the modified problem, this requires that only a simple summation be performed. The evidence presented thus far suggests that the summation over the fast and evanescent modes is equivalent to a numerical integration over the continuous spectrum in the corresponding original problem. In many cases, the resulting approximation to the contribution of the continuous spectrum is quite adequate and, hence, a straightforward application of the bounded approach is sufficient [7]. In other cases, such as in the example considered in the previous sections, a further numerical integration over a range of bound locations is necessary. The deciding factor seems to be the relative excitation of the lower part of the spectral range $0 \leq \beta \leq k_0$. If it is well excited, the highly dispersive nature of the fast modes (which causes the straightforward approach to be numerically impractical) conveniently allows the variable-bound approach to yield accurate results in a numerically more efficient manner. Essentially, the reason is the variable-bound approach allows better coverage of the fast and evanescent mode spectra and, hence, a more accurate numerical integration over the continuous spectrum is achieved.

III. TE- AND TM-MODE SCATTERING

Now, TE- and TM-mode scattering over a wide range of discontinuity parameters will be considered in order to illustrate the application of the variable-bound approach. Consideration of the TE-mode case allows a comparison

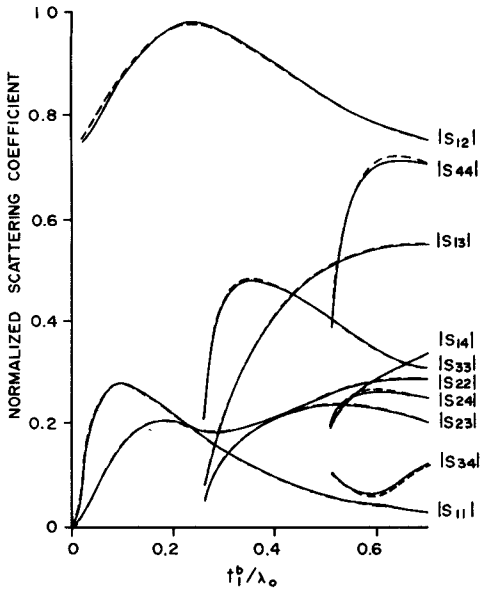

Fig. 6. TE-slow-mode scattering coefficients against t_1^b/λ_0: $\epsilon_r = 5.0$, $t_1^a = 0.2t_1^b$. —— variable-bound approach. – – – Rozzi's approach.

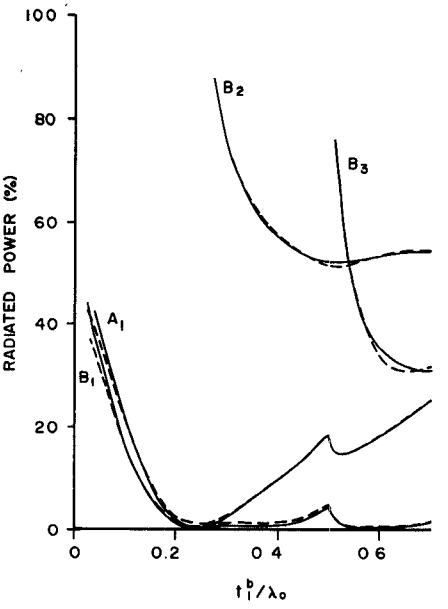

Fig. 7. Total normalized radiated power against t_1^b/λ_0 for TE-modes, same parameters as in Fig. 6.

with the results obtained using Rozzi's method while the TM-mode case is considered since no previous results are available (to the authors' knowledge).

A. TE-Mode Incidence

Referring to Fig. 1, the following parameters were chosen: $\epsilon_r = 5.0$, $t_1^a = 0.2t_1^b$, and an H-bound. The normalized slow-mode scattering coefficients are plotted (solid curves) in Fig. 6 as a function of t_1^b/λ_0. For convenience, the curves have been labeled with the standard scattering matrix notation where S_{ij} is the normalized scattering coefficient of the jth mode relative to the ith incident mode. The single slow mode in waveguide A is associated with subscript 1, whereas the first three slow modes in waveguide B are associated with subscripts 2, 3, and 4, respectively. The solid lines in Fig. 6 were calculated using the procedure outlined in Section II-C. In most cases, $N = 10$, $\delta t_{B0} = 0.1$, and Δt_{B0} defined over 0.9 to 1.4 were used. In a few instances, it was necessary to use $\delta t_{B0} = 0.05$ because of the large fluctuations of the coefficients (these instances were mainly associated with incidence of mode 2 from waveguide B), whereas, in other cases, ($t_1^b \ll \lambda_0$ or when the second and third slow modes in waveguide B were close to cutoff), $N = 15$ and a Δt_{B0} defined over 1.9 to 2.4 were necessary. The corresponding results for the total radiated power approximations, obtained by numerically integrating P_r over Δt_{B0}, are shown as the solid curves in Fig. 7. Curve A_1 denotes incidence of the first slow mode from waveguide A and curves B_1, B_2, and B_3, refer to incidence of the first three slow modes in waveguide B.

The dashed curves in Figs. 6 and 7 are the results calculated using Rozzi's method. For $t_1^b < 0.3\lambda_0$, sixth-order Laguerre polynomials were used, whereas for $t_1^b \geq 0.3\lambda_0$ tenth-order Laguerre polynomials were used. The excellent agreement between the solid and dashed curves in these figures confirms that the bounded approach is effectively a means of performing a numerical integration over the continuous spectrum in the original problem and apparently as accurate a means as that proposed by Rozzi. In this respect, Rozzi's method appears to require more Laguerre polynomials as the number of slow modes increased. Consequently, the computation time for the numerical integration over the continuous spectrum increased dramatically.[2] It is also worth mentioning at this point that the dashed curves in Fig. 7 were computed from the surface wave coefficients by assuming that power conservation held exactly. In the variable-bound approach, the radiated power is computed directly, maintaining the power conservation as a useful check. In order to do this using Rozzi's method, considerably more computation would be required.

B. TM-Mode Incidence

The variable-bound approach is applied equally well to the TM-mode case. This will be demonstrated by considering the same basic configuration as in the previous section but with an E-bound. The results for the slow-mode scattering coefficients are shown by the solid lines in Fig. 8 and those for the radiated power are shown in Fig. 9. The annotation on the curves in these figures is identical to that used in Figs. 6 and 7. In most cases, these results were calculated using $N = 15$, $\delta t_{B0} = 0.1$, and Δt_{B0} was defined over 0.9 and 1.4. As in the TE-mode case, $\delta t_{B0} = 0.05$ or $N = 20$ with Δt_{B0} defined over 1.9 to 2.4 were necessary in some cases. The dashed curves shown in these figures were calculated with $N = 40$, $\delta t_{B0} = 0.1$, and Δt_{B0} defined over

[2]The increase in the number of terms could be due to the requirement of higher order polynomials to account for the oscillations of the higher order surface wave mode fields in the dielectric. If so, the alternative sequence of expanding functions [5] as proposed by Rozzi may be more appropriate in such cases, although this has not been confirmed numerically.

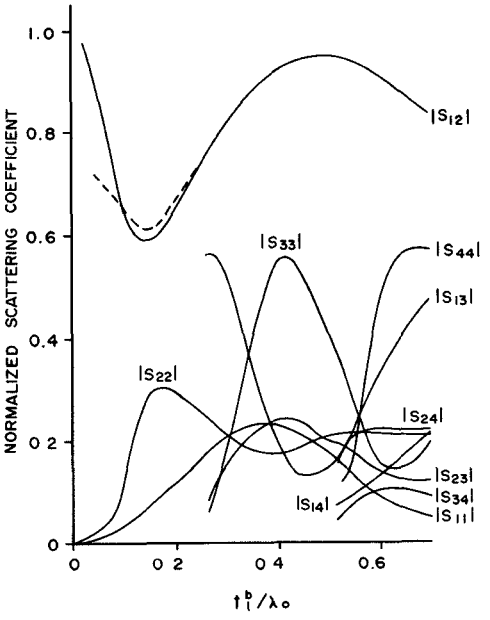

Fig. 8. TM-slow-mode scattering coefficients against t_1^b/λ_0 (variable-bound approach): $\epsilon_r = 5.0$, $t_1^a = 0.2t_1^b$. —— $N = 15$ with Δt_B over 0.9 to 1.4. - - - $N = 40$ with Δt_B over 3.9 to 4.4.

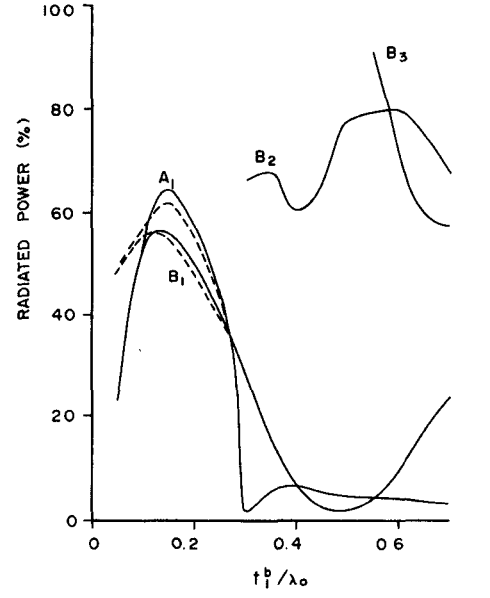

Fig. 9. Total normalized radiated power against t_1^b/λ_0 for TM-modes, same parameters as in Fig. 8.

3.9 to 4.4. The reason for the discrepancy between the solid and dashed curves is the relatively large field extent of the TM-slow modes in waveguide A for $t_1 \ll \lambda_0$, as will be discussed in Section IV. The accuracy of the results shown in Figs. 8 and 9 is expected to be comparable to that in the TE-mode case—there are no other results to compare with.

It may be of interest to note that field singularities occur at the dielectric edges in the plane of the discontinuity for TM-modes but not for TE-modes. Consequently, to achieve comparable accuracy in applying the bounded approach, more modes are required for TM cases than the corresponding TE cases. Other similarities and differences between TE- and TM-mode scattering will be examined in the following sections.

IV. Mode Orthogonality and Scattering

To this point, it has been shown that the scattering by abrupt discontinuities on open dielectric waveguides may be evaluated accurately and with comparative ease using the variable-bound approach. In this section, the mechanism of the scattering process is examined in the context of individual mode interactions. In particular, the close and meaningful relationship between the scattering properties and the orthogonality of the modes will be shown. A mathematically precise statement of this relationship is given by (5) and (6). However, these equations are not easily interpreted in terms of individual modes. Thus, a different mathematical statement will be developed.

Using (3) and (4), the solutions to (1) and (2) may be expressed in the following form:

$$b_l = \frac{P_{il}^{ab} + P_{li}^{ba}}{2P_l^b} + \sum_{n=1}^{N} a_n \frac{P_{nl}^{ab} - P_{ln}^{ba}}{2P_l^b} \tag{13}$$

$$a_k = \sum_{m=1}^{N} b_m \frac{P_{mk}^{ba} - P_{km}^{ab}}{2P_k^a} \tag{14}$$

where $l, k = 1, \cdots, N$, and i denotes incident. Equations (13) and (14) link individual mode coefficients through inter-waveguide bi-orthogonality relations. This particular form of the equations was chosen because the first term in (13) represents a good approximation for the $\{b_l\}$. Hence, the following iterative solution presents itself: i) let the first order approximation be

$$a_k^{(1)} = 0 \tag{15}$$

$$b_l^{(1)} = \frac{P_{il}^{ab} + P_{li}^{ba}}{2P_l^b} \tag{16}$$

and ii) iterate

$$a_k^{(J+1)} = \sum_{m=1}^{N} b_m^{(J)} \frac{P_{mk}^{ba} - P_{km}^{ab}}{2P_k^a} \tag{17}$$

$$b_l^{(J+1)} = b_l^{(1)} + \sum_{n=1}^{N} a_n^{(J+1)} \frac{P_{nl}^{ab} - P_{ln}^{ba}}{2P_l^b},$$

$$l, k = 1, \cdots, N, J = 1, \cdots. \tag{18}$$

The mathematical implications of this iterative technique appear worthy of a separate investigation and are not considered here. The iterative scheme, however, provides a simple interpretation of the scattering process. Namely, the sequence of events which occur in the plane of the discontinuity is one in which the first-order scattering of the incident mode (i.e., (15) and (16)) is repeatedly adjusted by higher order scattering (successive iterations) until the boundary conditions are satisfied.

In order to test the validity of the above interpretation and to examine more closely the link between scattering and mode orthogonality, let us consider the first-order scattering approximation given by (16). The slow-mode

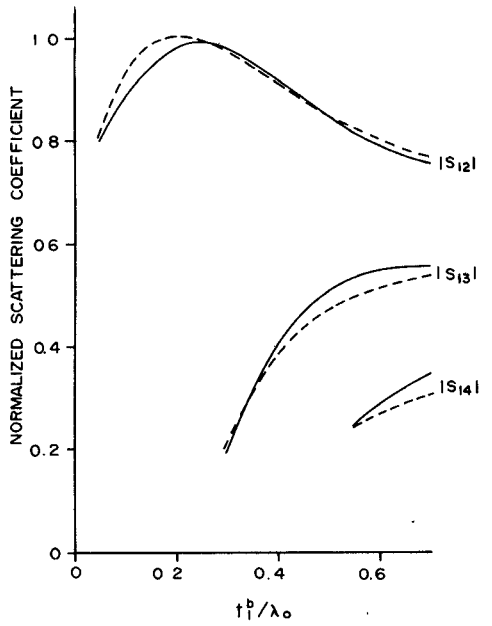

Fig. 10 TE-slow-mode transmission coefficients against t_1^b/λ_0 (with $N=10$): $\epsilon_r=5.0$, $t_1^a=0.2t_1^b$, $t_{B0}=4.0$. —— full solution. - - - first order scattering.

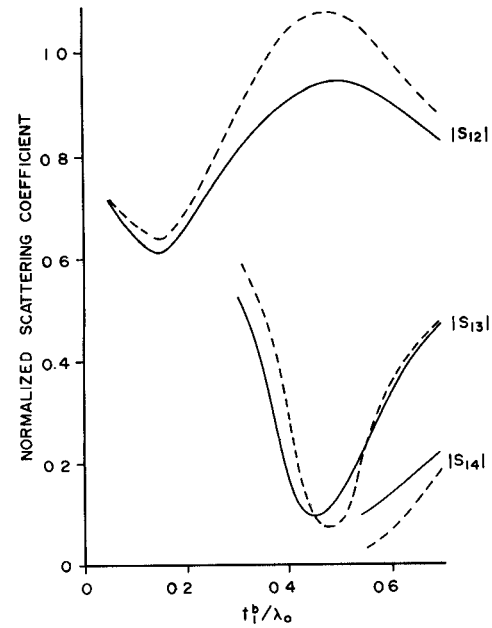

Fig. 11. TM-slow-mode transmission coefficients against t_1^b/λ_0, same parameters as in Fig. 10.

transmission coefficients corresponding to those shown in Figs. 6 and 8 are plotted versus t_1^b/λ_0 in Figs. 10 and 11, respectively. The solid curves were obtained from the full solution of (5) and (6), whereas the dashed curves represent the first-order approximation. For the purposes of this discussion all calculations were done using $t_{B0}=4.0$ (i.e., no averaging, thus the solutions will be somewhat different from those shown in Figs. 6–9). The results in Figs. 10 and 11 clearly indicate that (16), and hence the inter-waveguide bi-orthogonality, accounts for the general characteristics of the slow mode transmission coefficients in both the TE- and the TM-mode cases. The differences between the corresponding dashed and solid curves are a measure of the amount of readjustment (higher order scattering) required to satisfy the boundary conditions. In many cases, due to the exceptionally close agreement between the dashed and the solid curves, the scattering appears to be primarily of first order.

Equation (16) may also be used to generate first-order approximations to the transmitted radiated power by summing the powers in the fast-mode transmission coefficients. These results are shown as the dotted curves in Fig. 12(a) and (b) for TE- and TM-modes, respectively. Also shown in these figures are the curves (solid) for the total radiated power obtained from the full solution of (5) and (6). The notation on the solid curves is the same as that used in Figs. 7 and 9; corresponding dashed curves are denoted by the primed quantities. For reference, the results corresponding to those shown as B_3', but calculated from the full solutions, are indicated by the circles at selected points. As before, the results obtained using (16) give a good indication of the general characteristics of the full solution. Generally, cases where the dotted curves are much lower than the corresponding solid curves appear to occur because the first-order approximation does not account for reflected energy (see, for example, the curves B_3 and B_3'). On the other hand, cases where the dotted curves are much higher than the solid curves (i.e., B_2 and B_2' in Fig. 12(a)) are generally indicative of significant higher order scattering. Also, Fig. 12(a) and (b) appear to indicate that radiation is predominantly first order for the lowest order modes (both TE and TM).

Other interesting aspects of the scattering, over the range of discontinuities considered, may be inferred from Fig. 12(a) and (b). For example, both figures indicate that there is relatively little back radiation caused by the lowest order mode in waveguide A, whereas there is considerable back radiation caused by the third mode in waveguide B. In both the TE- and TM-mode cases, there is also significant higher order scattering associated with the incidence of the second slow mode in waveguide B.

In the previous discussion, the scattering behavior has been related to the inter-waveguide bi-orthogonality through the iterative scheme. It now remains to relate orthogonality to the field characteristics on a particular structure. Such a relationship would make it possible to predict and to qualitatively explain the scattering behavior of specific modes. In view of the type of guiding structure considered in this work, the field characteristics most closely associated with orthogonality is power concentration.

A parameter t_c may be defined as the value of x (see Fig. 1) such that 99.99 percent of the power in a mode is contained in the range $0 \leq |x| \leq t_c$. In Fig. 13, the values of t_c/λ_0 are plotted versus t_1/λ_0 for each of the first three modes in the waveguide considered. The solid curves represent TE-modes and the dashed curves represent TM-modes. For reference, the dielectric thickness is shown under the shaded area. The value of t_c effectively describes the field extent of the slow modes. Thus, as expected, Fig. 13 indicates that the slow modes tend to have their energy

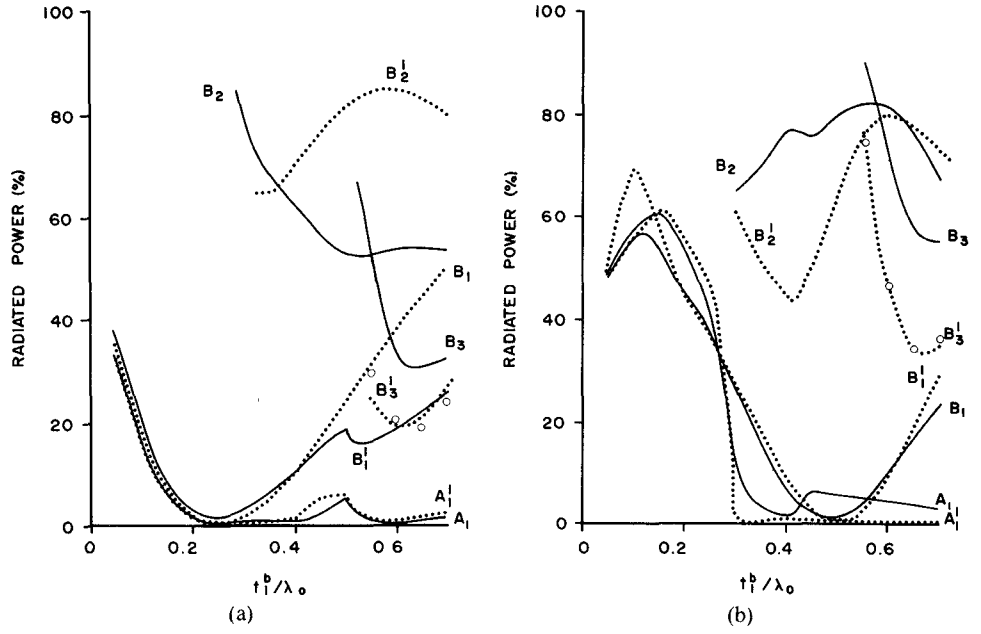

Fig. 12. (a) TE-modes. (b) TM-modes. $\epsilon_r = 5.0$, $t_1^a = 0.2t_1^b$, $t_{B0} = 4.0$. —— full solution for total (back and forward) power. o o o full solution for forward power. · · · first order forward power.

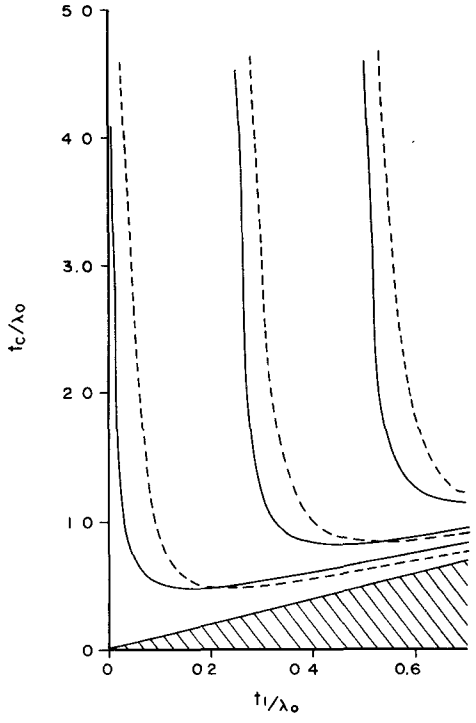

Fig. 13. Slow-mode power concentration against t_1/λ_0: $\epsilon_r = 5.0$. —— TE-modes. – – – TM-modes.

confined to the dielectric. The fast modes do not exhibit this behavior and, hence, a slow mode is expected to become more orthogonal to the fast modes on the other side of the discontinuity as t_c/λ_0 decreases. This simple argument accounts for several features of the curves shown in Figs. 10–12. It is perhaps most graphically demonstrated by curve A_1 in Fig. 12(a) which shows the radiation decreasing in the range $t_1^b \leq 0.20\lambda_0$. The corresponding range in waveguide A is $t_1^a \leq 0.04\lambda_0$ for which t_c/λ_0 is rapidly decreasing as shown in Fig. 13. Conversely, over the same range, the TM slow mode is never well confined and, therefore, curve A_1 in Fig. 12(b) indicates that much more radiation occurs in this case.

V. Conclusions

The main contribution of this work is the development of a unified approach (albeit approximate) for dealing with the problem of an arbitrary abrupt discontinuity on an open dielectric waveguide. This unification manifests itself in two aspects of the work. First, the link between the bounded and the corresponding unbounded problem for planar dielectric waveguides was more closely examined. It was shown that, by utilizing the dispersive properties of the mode spectra of the bounded waveguide, the variable-bound approach allows the complete mode spectra to be simply and accurately accounted for. Second, a link between scattering and inter-waveguide orthogonality was established. By interpreting the scattering in terms of a simple iterative scheme, it was shown that scattering may be classified as being of first or of higher order depending on the amount of readjustment needed to satisfy the boundary conditions in the plane of the discontinuity. Through orthogonality, scattering was also shown to be related, ultimately, to the physical characteristics of the mode fields.

Two types of examples were considered in order to demonstrate the application of the approach used in this work. Results for TE-mode propagation allowed a comparison with corresponding results obtained using Rozzi's method over a wide range of discontinuity parameters. Agreement to within 1 percent was achieved in most cases by using very modest numbers of modes ($N = 10$). Results for TM propagation were obtained with similar computational efficiency, also over a wide range of parameters and are believed to be of comparable accuracy. Both TE- and

TM-mode results appeared to confirm the simple interpretation of the scattering process based on mode orthogonality. This allowed similarities and differences between TE- and TM-mode scattering to be explained.

It is perhaps most significant that the evidence presented here indicates that, by appropriate consideration of the discrete mode spectra of the bounded waveguides, an accurate numerical integration over the continuous spectrum of the corresponding unbounded waveguide may be performed. This implies that the application of the present technique depends only upon the one-to-one correspondence of the bounded and unbounded mode spectra, and, hence, may be applied with confidence to all planar dielectric waveguide problems. Additional analysis, may be necessary for cylindrical structures [10], [11].

Appendix I

Mode Fields

Referring to Table I, the mode fields in the range $|x| \leq t_1$ are already cast in the same form (apart from a normalization constant) as those used for the corresponding unbounded structure [3], [5]. In the range $t \leq |x| \leq t_B$, e_y (and, hence, the other field components) may be written as

$$e_y = C\cos p_2(x - t_1 + t_1 - t_B)$$
$$= \cos p_1 t_1 \{\cos p_2(x - t_1) - \sin p_2(x - t_1)\tan p_2(t_1 - t_B)\}. \tag{19}$$

Now, using solutions of $F_E(\beta)$

$$e_y = \cos p_1 t_1 \cos p_2(x - t_1) - \frac{p_1}{p_2}\sin p_1 t_1 \sin p_2(x - t_1)$$
$$= C_e e^{jp_2 x} + C_e^* e^{-jp_2 x} \tag{20}$$

where

$$C_e = \tfrac{1}{2}e^{-jp_2 t_1}\left(\cos p_1 t_1 + j\frac{p_1}{p_2}\sin p_1 t_1\right). \tag{21}$$

Equations (20) and (21) are identical to those given by Marcuse [3] with B_e (his notation) equal to one. In a similar manner, (19) may be rearranged to give the form used by Rozzi [5]. Thus, at discrete values of β given by solutions of $F_E(\beta)$, the fields of the fast and the evanescent modes are identical to the fields of the continuous spectrum modes of the corresponding unbounded waveguide over the range $|x| \leq t_B$.

For the slow modes, p_2 is imaginary, and, hence, in the range $t_1 \leq |x| \leq t_B$, e_y may be written as

$$e_y = \cos p_1 t_1 \frac{\cosh \gamma_2(x - t_B)}{\cosh \gamma_2(t_1 - t_B)} \tag{22}$$

where $p_2 = j\gamma_2$. Now, in the limit as $t_B \to \infty$

$$e_y = \cos p_1 t_1 e^{-\gamma_2(x - t_1)}. \tag{23}$$

Equation (23) can be recognized as the form for a surface wave mode field. Furthermore, the limiting form of $F_E(\beta)$ is given by

$$p_1 \tan p_1 t_1 = \gamma_2 \tag{24}$$

TABLE V
TE-Modes— *H*-Bound

$P^{ab}_{nm} - \beta^b_m P^{ba}_{mn}/\beta^a_n$		
	$t_1^a < t_1^b$	$t_1^a > t_1^b$
B	β_m^b	β_m^b
I_1	T_1	T_1'
I_2	$C_n^a T_{2C}$	$C_m^b T_{2C}'$
I_3	$C_n^a C_m^b T_{3C}'$	$C_n^a C_m^b T_{3C}$

TABLE VI
TM-Modes— *E*-Bound

	P^{ab}_{nm}		P^{ba}_{mn}	
	$t_1^a < t_1^b$	$t_1^a > t_1^b$	$t_1^a < t_1^b$	$t_1^a > t_1^b$
B	β_n^a	β_n^a	β_m^b	β_m^b
I_1	$T_1\delta_R$	$T_1'\delta_R$	$\delta_R T_1$	$\delta_R T_1'$
I_2	$C_n^a T_2$	$C_m^b T_2'\delta_R$	$C_n^a T_2\delta_R$	$C_m^b T_2'$
I_3	$C_n^a C_m^b T_3'$	$C_n^a C_m^b T_3$	$C_n^a C_m^b T_3'$	$C_n^a C_m^b T_3$

which is the characteristic equation for the surface wave modes on the corresponding unbounded structure. Thus, the slow modes correspond identically to surface wave modes in the limit as $t_B \to \infty$. A similar analysis holds for TM-modes.

Appendix II

Expressions for P_n^a, P_n^b, P_{nm}^{ab}, and P_{mn}^{ba}

In this section, the following functional relationships are maintained:

$$Sa(x) = \frac{\sin x}{x} \tag{25}$$

$$\delta_k = \eta_0/k_0, \quad \text{(TM-modes)}$$
$$= 1/k_0\eta_0, \quad \text{(TE-modes)} \tag{26}$$

$$\delta_R = 1/\epsilon_r, \quad \text{(TM-modes)}$$
$$= 1, \quad \text{(TE-modes)}. \tag{27}$$

The values of P_n^a and of P_n^b (n is the mode order) can be computed from

$$P_n' = \tfrac{1}{2}\beta_n'\delta_k\{\delta_R t_1'[1 + Sa(2p_{1n}'t_1')]$$
$$+ (C_n')^2[1 + Sa(2p_{2n}'(t_1' - t_b))]\} \tag{28}$$

where the primed quantities are to be associated with superscript a for P_n^a and b for P_n^b and where C_n' can be found in either Table I or Table II.

The values of P_{nm}^{ab} and P_{mn}^{ba} can be computed from the following expression:

$$P = \tfrac{1}{2}\beta\delta_k[I_1 + I_2 + I_3] \tag{29}$$

where β, I_1, I_2, and I_3 are defined in Tables V and VI.

In the above tables

$$T_1 = t_1^a\{Sa[(p_{1n}^a + p_{1m}^b)t_1^a] + Sa[(p_{1n}^a - p_{1m}^b)t_1^a]\} \quad (30)$$

$$T_2 = \frac{\sin A_1 - \sin A_2}{p_{2n}^a + p_{1m}^b} + \frac{\sin A_3 - \sin A_4}{p_{2n}^a - p_{1m}^b} \quad (31)$$

$$T_3 = -(t_1^a - t_B)\{Sa[(p_{2n}^a + p_{2m}^b)(t_1^a - t_B)] + Sa[(p_{2n}^a - p_{2n}^b)(t_1^a - t_B)]\} \quad (32)$$

where

$$A_1 = (p_{2n}^a + p_{1m}^b)t_1^b - p_{2n}^a t_B$$
$$A_2 = (p_{2n}^a + p_{1m}^b)t_1^a - p_{2n}^a t_B$$
$$A_3 = (p_{2n}^a - p_{1m}^b)t_1^b - p_{2n}^a t_B$$
$$A_4 = (p_{2n}^a - p_{1m}^b)t_1^a - p_{2n}^a t_B.$$

Expressions for T_1' and T_3' can be obtained from T_1 and T_3, respectively, by substituting t_1^b for t_1^a. Expressions for T_2' can be obtained from T_2 by interchanging superscripts a and b.

Acknowledgment

The authors wish to thank Dr. M. J. Wilmut of Royal Roads Military College and Dr. R. F. MacKinnon of the Defence Research Establishment Pacific for many helpful discussions concerning this work.

References

[1] P J. B. Clarricoats and A. B. Sharpe, "Modal matching applied to a discontinuity in a planar surface waveguide," *Electron. Lett.*, vol 8, pp. 28–29, Jan. 1972.

[2] G. A. Hockham and A. B. Sharpe, "Dielectric-waveguide discontinuities," *Electron. Lett.*, vol 8, pp. 230–231, May 1972.

[3] D Marcuse, "Radiation losses in tapered dielectric slab waveguides," *Bell. Syst. Tech. J.*, vol. 49, pp. 273–290, Feb. 1970.

[4] S. F. Mahmoud and J C. Beal, "Scattering of surface waves at a dielectric discontinuity on a planar waveguide," *IEEE Trans. Microwave Theory Tech* , vol. MTT-23, pp. 193–198, Feb 1975.

[5] T. E. Rozzi, "Rigorous analysis of the step discontinuity in a planar dielectric waveguide," *IEEE Trans. Microwave Theory Tech.*, vol. MTT-26, pp. 738–746, Oct. 1978.

[6] A D. Yaghjian and E T. Kornhauser, "A modal analysis of the dielectric rod antenna excited by the HE_{11} mode," *IEEE Trans Antennas Propagat.*, vol. AP-20, pp 122–128, Feb. 1972.

[7] G. H. Brooke and M M. Z Kharadly, "Step discontinuities on dielectric waveguides," *Electron. Lett.*, vol. 12, pp. 473–475, Sept. 1976.

[8] G. H Brooke and W. K. McRitchie, "Effect of dielectric edge conditions on mode-matching solutions," *Electron. Lett* , vol. 11, pp 422–423, Aug 1975.

[9] P. H Masterman and P. J B. Clarricoats, "Computer field-matching solution of waveguide transverse discontinuities," *Proc. Inst Elec Eng.*, vol. 118, pp 51–63, Jan. 1971.

[10] P. J. B. Clarricoats, "Backward waves in waveguides containing dielectric," *Proc. Inst. Elec. Eng* , vol. 108 C, pp. 496–501, 1961.

[11] P. J. B. Clarricoats and J M. W. McBride, "Properties of dielectric-rod junctions in circular waveguide," in *Proc. Inst Elec. Eng.*, vol 111, pp 43–50, Jan. 1971

G. H. Brooke, photograph and biography not available at the time of publication

M. M. Z. Kharadly, photograph and biography not available at the time of publication